LA-UR- 98-45

Title:

ACTIVE CONTROL OF 2/1 MAGNETIC ISLANDS IN THE HBT-EP TOKAMAK

Author(s):

G.A. Navratil, Columbia University
C. Cates, Columbia University
M.E. Mauel, Columbia University
D. Maurer, Columbia University
D. Nadle, Columbia University
E. Taylor, Columbia University
Q. Xiao, Columbia University
G. A. Wurden, P-24
W. A. Reass, LANSCE-5

Submitted to:

APS
November 18-21, 1997
Pittsburgh, PA
Submittal to: Physics of Plasmas

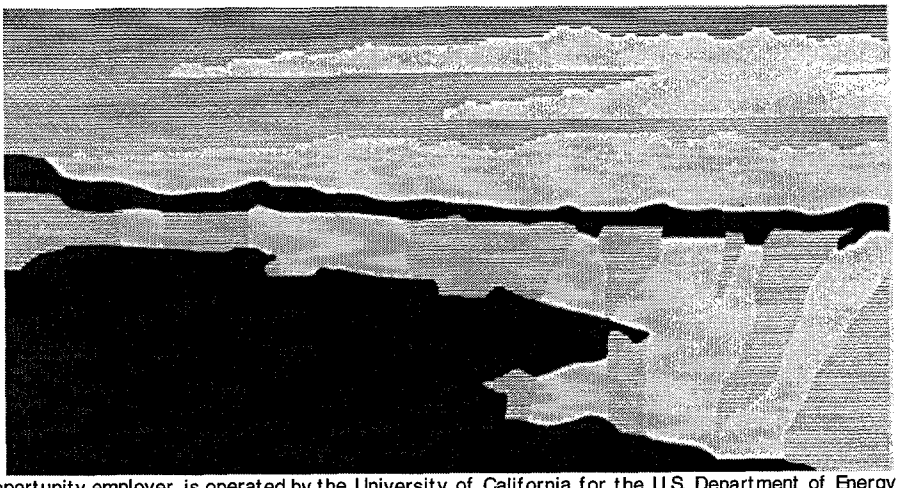

Los Alamos
NATIONAL LABORATORY

Form No. 836 R5
ST2629 10/91

DISCLAIMER

DISCLAIMER

Portions of this document may be illegible in electronic image products. Images are produced from the best available original document.

FINAL SUBMITTED VERSION

Active control of 2/1 magnetic islands in the HBT-EP tokamak

G. A. Navratil, C. Cates, M. E. Mauel, D. Maurer, D. Nadle, E. Taylor, and Q. Xiao
Department of Applied Physics
Columbia University
New Your, NY 10027

W. A. Reass and G. A. Wurden
Los Alamos National Laboratory
Las Alamos , NM 87545

Closed and open loop control techniques were applied to growing $m/n = 2/1$ rotating islands in wall stabilized plasmas in the HBT-EP tokamak. The approach taken by HBT-EP combines an adjustable segmented conducting wall (which slows the growth or stabilizes ideal external kinks) with a number of small (6° wide) saddle coils located between the gaps of the conducting wall. In this paper we report demonstration of 2-phase island rotation control from 5 kHz to 15 kHz and observation of the phase instability which are well modeled by the single-helicity, predictions of nonlinear Rutherford island dynamics for 2/1 tearing modes including important effects of ion inertia and FLR which appears as a damping term in the model equations. The closed loop response of active feedback control of the 2/1 mode at moderate gain was observed to be in good agreement with the theory. We have also demonstrated suppression of the 2/1 island growth using an asynchronous frequency modulation drive which maintains the flow damping of the island by application of rotating control fields with frequencies alternating above and below the natural mode frequency. This frequency modulation control technique was also able to prevent disruptions normally observed to follow giant sawtooth crashes in the plasma core.

I. INTRODUCTION

Economically attractive, steady state fusion power-plant designs based on advanced tokamak physics emphasize a combination of three important features: (i) high beta, (ii)

large and well aligned non-inductive bootstrap current to permit economic, steady state operation, and (iii) good confinement. The prospects for improved confinement in magnetically confined toroidal fusion plasmas has made substantial progress moving from the H-mode of the early 80's to the VH-mode in the early 90's to the recent use of ExB shear to suppress turbulence in the plasma core and reduce the level of ion transport to neoclassical values in most of the plasma volume[1]. However, high beta plasmas with well aligned bootstrap current require operation at levels of $\beta_N = 10^{-8}\ \beta aB/I_p$ well above the beta limit for the low-*n* ideal kink mode.[2,3] The most promising approach to stabilize the low-*n* ideal kink mode is the use of a close fitting conducting wall which, if perfectly conducting, has been predicted to improve the no-wall beta limit by factors of more than three.[2,3] Experimental studies have shown that the no-wall beta limit can be exceeded by modest factors in experiments on DIII-D[4] and on HBT-EP[5], however, slower growing modes are observed to set a lower beta limit in these wall-stabilized plasmas. The two most important of this class of slower growing modes are the resistive wall mode[6] (RWM) which has a growth rate slowed to the resistive wall time constant and is an external mode (since its resonant surface lies in the vacuum region outside the plasma edge), and resistive tearing modes which develop large magnetic islands resonant on magnetic surfaces inside the plasma. The most dangerous of these internal modes is the m/n = 2/1 tearing mode and associated magnetic island, since this mode has been found to play an important role in the tokamak current disruption process. However, since these residual modes have much slower time-scales than the ideal hydrodynamic time scale for growth, they are in principle able to be actively controlled.

II. MODE CONTROL SYSTEMS AND BASIC PARAMETERS OF HBT-EP

The approach to mode control in HBT-EP consists of a combination of active and passive stabilization techniques. A 10 segment, adjustable conducting wall is used to

provide passive stabilization of the low-n ideal kink mode. Active control of the residual slower growing modes is effected by applications of rotating helical magnetic field perturbations generated by highly modular saddle coils external to the vacuum vessel. This configuration is shown schematically in Fig. 1. The toroidal plasma has an aspect ratio, R/a = 6 with R = 0.92 meters. The passive stabilizing conducting wall consists of ten, 1 cm thick aluminum segments, each of which covers 26° of toroidal angle. These wall segments can be varied in radial position to study the effect of wall proximity on kink mode stabilization and these results have been published previously.[5,7] In the experiments reported in this paper on active mode control, the wall segments were positioned less than 10% of the plasma minor radius from the plasma edge for maximum passive stabilization of the ideal time scale modes.

At four of the 10° wide gaps in the conducting wall segments are located m=2 saddle coils. Each of these saddle coils is 6° wide in toroidal angle and positioned in poloidal angle to couple optimally to an m=2, n=1 helical field. The saddle coils project a radial field into the plasma through 10 cm wide quartz toroidal gaps that allow efficient penetration of magnetic perturbations with frequencies up to 20 kHz. This highly modular configuration only covers about 3% of the toroidal surface surrounding the plasma.

Two of these saddle coils are connected in series and driven with a 10 MW linear amplifier to provide a $\sin(\omega t+\delta)$ response field and the other two coils are connected in series and driven with an independent 10MW linear amplifier to provide a $\cos(\omega t+\delta)$ response field; together these coils provide a 2-phase, quadrature winding to producing a rotating magnetic perturbation, as shown schematically in Fig. 2. The 10 MW linear amplifiers used in these experiments have a bandwidth greater than 25 kHz and can deliver ±600 Amperes through each of the 9-turn saddle coils. The phase and amplitude information from the rotating 2/1 island structure in the plasma is obtained from a set of $\sin 2\theta$ and $\cos 2\theta$ Rogowski coils which are physically remote (as shown in Fig 1) from the saddle coil response fields and have very low direct pick-up. For closed loop, active mode

control experiments, these sin2θ and cos2θ signal measurements are digitized by a digital signal processor (DSP) at 100 kHz and in real time (Δt=10 μsec) phase shifted and gain adjusted to drive the input stages of the two 10MW linear amplifiers which provide the sine and cosine quadrature response fields that are fed back to the rotating 2/1 islands in the plasma.

The basic parameters of the HBT-EP tokamak are summarized in Table I. For these experiments on 2/1 mode control, the edge q value was maintained near $q \sim 2.5$ and held to values less than 3. This type of plasma produced strong naturally occurring 2/1 mode activity that began about 3 msec after plasma formation and which always led to a hard plasma disruption. The typical disruption sequence included large growth of the 2/1 islands immediately following a large sawtooth crash at about 7 msec after plasma formation resulting in prompt (< 100 μsec) loss of central temperature and significant density loss followed by a collapse of the plasma current over the following 0.5 msec. These plasmas provided a period of relativly constant amplitude saturated 2/1 activity from 3 msec to 7 msec and then presented a strong disruption challenge to test the robustness of any mode control scheme applied to the discharge.

Table I

Major radius, R_o	0.92-0.97 meters
Minor radius, a	0.15-0.19 meters
Plasma Current, I_p	≤ 25 kA
Toroidal Field, B_T	≤ 0.35 Tesla
Pulse length	10 msec
Electron temperature, T_e	≤ 80 eV average
Density, n_e	~ 1 x 10^{19} m^{-3}

III. ROTATING ISLAND MODEL EQUATIONS

To analyze our results we use the non-linear, single helicity model which has been built up over many years[8,9,10,11,12] to explain the interaction of external magnetic perturbations and a saturated tearing mode which appears as a set of rotating magnetic islands on the resonant surface in the plasma. Normalizing the mode amplitude, b, and rotation frequency, Ω, the simplified set of coupled dynamical equations for b and Ω used to model the mode control experiments described in this paper are given by,

$$\frac{db}{dt} = g_1\left(1 - \sqrt{b}\right)\sqrt{b} + g_2\frac{b_d}{\sqrt{b}} - g_3\frac{(\Omega - 1)^2}{b} \tag{1}$$

$$\frac{d\Omega}{dt} = -h_1(\Omega - 1) + h_2\, b_q\, b - h_3\frac{\Omega\tau_{wall}}{m^2 + (\Omega\tau_{wall})^2}b^2 \tag{2}$$

where, g_1, g_2, g_3, h_1, h_2, and h_3 are constants; $b \equiv (W/W_{sat})^2$ with W_{sat} defined as the saturated island width; $\Omega \equiv (\omega/\omega_o)$ where ω_o is the saturated island rotation frequency (which we take to be roughly the ExB toroidal rotation frequency which is in the electron diamagnetic drift direction). The direct drive term which either increases or decreases the mode amplitude, b_d, is proportional to $I_{coil}\cos(\delta)$ and the quadrature drive term is proportional to $I_{coil}\sin(\delta)$ with

$$\delta \equiv \delta_o + \int_0^t dt'(\omega - \omega_{coil}),$$

where δ is the phase relation between the rotating island at frequency ω, and the externally applied field, ω_{coil}. The first terms in Eqs. (1) and (2) describe the Rutherford growth term which leads to a saturated amplitude and frequency which in equilibrium are both normalized to unity. The second terms in Eqs. (1) and (2) are the direct drive and quadrature drive respectively which describes the interaction between the applied rotating helical perturbation field and the rotating 2/1 islands. The third terms include the most

important damping terms needed to fit the observed behavior of the active control experiments in HBT-EP. In Eq. (2) this damping is a wall drag term which is small since $\Omega\tau_{wall} \sim 80$ in for HBT-EP with $\Omega \sim 6 \times 10^4$ sec^{-1}. In Eq. (1) this third term describes damping or stabilizing of the mode amplitude due to ion inertia and FLR effects (see Ref. 12) and is quadratic in the rotation velocity difference between the island and background plasma fluid. This ion inertial stabilizing effect reduces the mode amplitude whenever the island moves faster or slower than the background plasma toroidal rotation velocity. While not previously considered in earlier active mode control experiments, we find this term to be significant in affecting the transient island dynamics in response to external perturbations.

IV. DRIVEN TOROIDAL ROTATION OF 2/1 ISLANDS

To benchmark the model described in Section III for application to the control coil geometry of HBT-EP, a series of open loop frequency ramp-up and ramp-down experiments was carried out. The results of a typical frequency ramp-up experiment are shown in Fig. 3. In this example we apply a sinusoidal current to the saddle coils and linearly advance the frequency from 2 kHz to 15 kHz over a period of 2 msec. The phase difference between the applied magnetic field and the field of the 2/1 rotating island is shown in the figure and indicates that as the rising frequency of the applied field approaches the natural frequency of the island rotation (~8 kHz), the mode decelerates and 'locks' to the rotating applied field at about 5 kHz. The 2/1 island is then accelerated up to about 14 kHz toroidal rotation frequency at which time the lock is lost. The phase difference between the driving field and mode field slowly advances from negative values to positive values as the torque demands on the driving field changes from retarding the rotation to accelerating the rotation as was reported in similar experiments on DITE.[9]

During the frequency ramp-up and frequency ramp-down experiments, the local ion flow velocity was measured with a local Langmuir Mach probe which measures the ion

fluid flow velocity near the 2/1 island. The results of this measurement are shown in Fig. 4 for both frequency ramp-up and ramp-down discharges. The ion fluid is observed to normally have a toroidal flow velocity near 0 prior to mode lock, which is consistent with the picture that the ion fluid is nearly stationary due to the large charge exchange viscosity on neutrals near the plasma edge, while the mode travels with the toroidal ExB drift velocity in the electron diamagnetic drift direction. In the case of the frequency ramp-up experiment of Fig 4, the ion fluid flow velocity drops to - 1kHz when the mode frequency locks on to the applied field at 5 kHz and is accelerated to a value somewhat above 0 as the mode is accelerated to near 14 kHz. The reverse is seen with the frequency ramp-down case: the ion fluid is accelerated from near 0 when the mode locks on to applied field at 14 kHz to somewhat below - 1 kHz as the mode is decelerated to 5 kHz. After mode lock is lost, the ion fluid returns to near 0 toroidal velocity in a few tenths of a msec. The ion fluid acceleration rate is seen here to be only about 20% of the mode acceleration rate, which is consistent with previous observations of this effect in Compass with application of a static external field[13] and on JFT-2M with a rotating applied field.[14]

At the time the external field is applied in the ramp-up experiment of Fig. 3, the mode rotation frequency is briefly driven up to a large value and then relaxes back to its normal equilibrium value prior to mode lock to the applied field. We note that this kick upward in frequency is accompanied by a decrease in the mode amplitude. A similar event occurs during the loss of mode lock with a rapid drop to 7 kHz and return to near 15 kHz which is accompanied by a drop in mode amplitude. This effect has been modeled as shown in Fig. 5 both with and without the ion inertia flow damping term in the model equations. In the case without the flow damping term included in the model, the mode is always found to lock onto the applied field and smoothly accelerate. In the case including the flow damping term, the phenomenon of a frequency excursion with associated mode amplitude reduction could be simulated, indicating that this term may play a role in the island dynamics.

V. STUDY OF THE PHASE INSTABILITY

When the phase of an applied external field rotating with a 2/1 island is maximally stabilizing in Eq. (1), the phase of the mode relative to the applied field is in an unstable equilibrium and is subject to an unstable growth of this phase difference called the phase instability.[15] This instability can be produced in HBT-EP by applying an external 2/1 field perturbation rotating at a frequency near to the natural 2/1 island rotation frequency. The islands will immediately lock on to the applied field and grow in amplitude to a new large saturated level. If at a pre-determined time, the phase of the applied field is suddenly advanced by 180°, the islands will now experience an applied external field which is stabilizing, resulting a reduction in the mode amplitude and in a rapid advance in the phase of the islands in response to phase instability as the islands again move into a condition of phase lock and amplitude growth. This technique for inducing the phase instability has been employed in HBT-EP and is shown in Fig. 6 together with 2 model simulations using Eqs. (1) and (2), one with and one without the ion inertial sheared flow damping term. Immediately after the phase change, there is a large decrease in the mode amplitude which we are unable to account for in the model if the ion inertia flow stabilizing term is not included. The large frequency increase of the mode as its phase advances to re-establish a phase-lock with external rotating 2/1 field, causes a significant decrease in mode amplitude induced by this stabilizing effect.

VI. ACTIVE FEEDBACK CONTROL

By applying a rotating external 2/1 field which is maintained in a stabilizing phase relation with the mode, it is possible to used a closed loop system to carry out active feedback suppression of the 2/1 island amplitude as was first demonstrated in DITE.[9] In the work reported here we carry out similar experiments, but using the highly modular saddle coil set described in Sec. II and implemented with a fast digital signal processor the

feedback scheme proposed[16] for use on JET. As discussed earlier in reference to Fig 2, the quadrature detection scheme on HBT-EP measures a sin2θ and cos2θ signal giving a phase and amplitude reference for closed loop active feedback. These sin2θ and cos2θ signals are digitized at a 100 kHz rate and processed by a digital signal processor to generate a phase shifted waveform that drives the high power amplifiers and applies a 2/1 rotating applied field with a predetermined phase shift with respect to the rotating islands. The feedback control algorithm implements a simple rotation matrix:

$$\begin{bmatrix} I_{cos}(t+\Delta t) \\ I_{sin}(t+\Delta t) \end{bmatrix} = G \begin{bmatrix} \cos(\delta) & -\sin(\delta) \\ \sin(\delta) & \cos(\delta) \end{bmatrix} \cdot \begin{bmatrix} B_{cos2\theta}(t) \\ B_{sin2\theta}(t) \end{bmatrix} \quad (3)$$

This scheme is designed to maintain a constant phase relation between the detected mode phase and applied external rotating field.

We can model the expected equilibrium response of the 2/1 islands by setting the time derivatives to 0 in Eqs. (1) and (2). Assuming that $\Omega\tau_{wall} >> 1$ we solve the following coupled non-linear equations for the expected mode amplitude and frequency as a function of phase angle and closed loop system gain, G.

$$0 = g_1\left(1 - \sqrt{b}\right)\sqrt{b} + g_2 G\cos(\delta)\sqrt{b} - g_3\frac{(\Omega - 1)^2}{b} \quad (4)$$

$$0 = -h_1(\Omega - 1) + h_2 G \sin(\delta) b - \frac{h_3 b^2}{\Omega\tau_{wall}} \quad (5)$$

Assuming moderate system gain the variation expected in Ω and b are plotted in polar form for variations in δ in Fig. 7. The mode is reduced in amplitude for $\delta = 0°$ and driven to larger amplitude for $\delta = 180°$. For phase angles of 90° and 270° the amplitude is little changed, but we expect a higher frequency at $\delta = 90°$ and a lower frequency when $\delta =$

270°. If the normalized mode frequency is reduced to values about 0.5, the mode is predicted to lock. This effect is most likely at about 230° and has been observed in the experiments as the gain is made larger.

Closed loop experiments were carried out for $\delta = 0°$ and 180° on a single discharge with the stabilizing phase angle applied for 1 msec followed by the destabilizing phase angle applied for the following 1 msec. These results are shown in Fig. 8 showing the time history of the applied phase angle, δ, the amplitude of the sine and cosine phase of the 2/1 islands, and the frequency of the island rotation. During the 1 msec application of the stabilizing phase angle, the frequency is observed to rise from about 7 kHz to 10 kHz with a relatively constant amplitude. After the transition to the destabilizing phase angle, the mode amplitude is observed to grow larger and the frequency of the mode is observed to decline from 10 kHz to 7 kHz in agreement with the expectations of the equilibrium model of Eqs. (4) and (5). If the data is averaged over 0.1 msec intervals and plotted against the predictions of the model, we find reasonably good agreement as also shown in Fig. 8.

A similar experiment can be carried out for the phase angles $\delta = 270°$ and 90° where we expect a frequency decrease and frequency increase. The results of this experiment are shown in Fig. 9. During the initial application of the frequency decrease phase angle, we see the frequency maintained at about 7 kHz. After the transition to the frequency increase phase angle, the island rotation frequency is observed to increase to about 9 kHz over 1 msec. These results are also plotted averaged over 0.1 msec intervals against the model predictions showing good agreement.

When the gain of the feedback system is increased to achieve a larger suppression of the mode amplitude or to attempt to control the 2/1 island size immediately prior to the normal strong growth phase prior to disruption, we find that phase accuracy of the response field is degraded and the closed loop system is no longer able to maintain a specified stabilizing phase angle. This effect appears to be due to the large phase angle delay inherent in the system using a 100 kHz digitization rate and a 10 μsec delay in

computing the next waveform update. The zero order hold digital delay used on the output combined with the 100 kHz data acquisition rate, results in a frequency dependent phase delay of more than 50°. Given the higher growth rate for the phase instability as the system gain is increased as well as the large frequency changes which can occur as the mode amplitude grows prior to disruption, the 100 kHz digital signal processing system was unable to maintain phase lock on the mode. As expected in light of the difficulties in maintaining a phase reference for the applied external rotating 2/1 field, tests of the system at high gain during the period of large 2/1 island growth immediately prior to disruption showed no effect on the disruption timing or severity.

VII. FREQUENCY MODULATION STABILIZATION

Since we have observed in the frequency ramp and phase instability model benchmark experiments described in Sec. IV and V, a significant role played transiently by ion inertia flow stabilization in reducing the island amplitude, experiments were carried out to induce this effect over a extended period. The use of time averaged flow stabilization to control the average mode amplitude was originally proposed by Kurita, et al.[17] who simulated the effect of modulation of an applied external rotating resonant field whose frequency was modulated alternately above and below the normal mode rotation frequency. Since the response of the rotating island to such an external field is to increase or decrease the rotation frequency in order to establish a phase lock on the applied field, this should result in a reduction in the mode amplitude during the periods where the $(\Omega-1)^2$ ion inertia flow damping term in Eq. (1) becomes large. By choosing the duration of the alternating high and low frequency periods to be sufficiently short so that mode lock is avoided, a time average reduction in the 2/1 island amplitude should be obtained. Shown in Fig 10 are the results of a simulation of this effect using parameters in the model Eqs. (1) and (2) which were benchmarked against the previous frequency ramp, phase instability, and active feedback experiments. Assuming a normal island rotation frequency of 10 kHz, a 2/1

rotating field was applied with a frequency of 15 kHz alternating with 5 kHz every 0.2 msec. We can see from the results of the simulation, that if the ion inertia flow stabilization term is not included in the model, the mode rapidly locks onto to the applied field and grows to relatively large amplitude. On the other hand, when this stabilizing term is included, the islands do not achieve phase lock and the mode amplitude is observed at a much lower average amplitude.

The frequency modulation stabilization experiment modeled above was carried out in HBT-EP and the results are summarized in Fig. 11. Shown in the figure is the application of the alternating 5 kHz and 15 kHz externally applied 2/1 drive field together with the response of the island rotation frequency. As the frequency of the applied field alternates, the rotating island toroidal velocity is strongly modulated and a phase lock with the applied field is avoided. Also plotted in Fig. 11 is the $(\Omega-1)^2$ ion inertia flow damping term based on the actual mode rotation frequency. During times when the values computed for $(\Omega-1)^2$ are relatively large are compared with the measured 2/1 island amplitude they are found to correlate with a reduction in mode amplitude.

Most significantly, when this frequency modulation stabilization technique is applied at the end of the discharge when the development of very large sawteeth normally leads to a hard disruption, the hard disruption was prevented and the discharge lifetime was extended. These results are shown in Fig. 12 for two discharges with edge $q \sim 2.5$, one with the frequency modulation stabilization applied and a very similar reference shot without frequency modulation stabilization. In the case of the reference shot 16389, we see that central soft x-ray emissivity rises in time until a very large sawtooth collapse occurs at about 6.6 msec with an associated loss of half the line integrated plasma density, and disruption of the plasma current which begins to collapse immediately. When the frequency modulation stabilization was applied in shot 16411 for a 3 msec period beginning at 4.5 msec, we see that this discharge also suffers a large sawtooth collapse at about the same time as the reference shot 16389, however, in this case the plasma density

and plasma current continue with little or no effect. This appears to be due to preserving the integrity of the outer flux surfaces by frequency modulation control of the 2/1 island size. The plasma core temperature begins to recover after the sawtooth collapse and a second large sawtooth event occurs again without loss of outer flux surface confinement or disruption of the plasma current.

The frequency modulation stabilization is turned off at 7.5 msec and 0.1 msec later the plasma suffers a hard disruption of the current and loss of plasma density. In contrast to the usual disruption sequence for these plasmas which initiate with a large central collapse of the soft x-ray emissivity, followed by growth of the 2/1 islands and then current disruption, in this frequency modulation stabilized plasma the current and density loss disruption actually precedes the central soft x-ray collapse, indicating the disruption event was initiated by loss of outer flux surface confinement shortly after the frequency modulation was switched off.

VIII. SUMMARY AND DISCUSSION

Closed and open loop control techniques were applied to growing m=2, n=1 rotating islands in wall stabilized plasmas in the HBT-EP tokamak. The approach taken by HBT-EP combines an adjustable segmented conducting wall (which slows the growth or stabilizes ideal external kinks) with 4 highly modular (6° wide) saddle coils located between the gaps of the conducting wall and covering only about 3% of the plasma surface. The success of these experiments provides a basis for consideration of systems with greater modularity and localization . The installation of extensive internal coils sets in larger tokamaks is technically difficult and the higher frequency response coils needed for control of internal modes prevents their location behind passive stabilization structures needed to deal with low-n deal kink modes. The option of a highly modular configuration in conjunction with a segmented passive stabilizer may allow the possibility of active control

of internal and external modes on medium scale experiments such as DIII-D and NSTX and even in larger scale devices like ITER.

In this paper we described experiments which demonstrate 2-phase island rotation control from 5 kHz to 15 kHz and the observation of the phase instability, both of which are well modeled by the single-helicity, predictions of nonlinear Rutherford island dynamics for 2/1 tearing modes. These model equations include important effects of ion inertia and FLR which appears as a quadratic flow damping term scaling like $(\Omega\text{-}1)^2$ for the mode amplitude. We find this to be an important term in modeling the observations of driven rotation and the phase instability. Induced ion flow was observed with local Langmuir Mach probes during the 2-phase island rotation drive experiments with the rate of ion fluid acceleration equal to about 20% of the rate of the island acceleration. The normal ion fluid flow velocity is nearly 0 and rotation rates somewhat larger than -1 kHz were measured relative to the island rotation direction.

The closed loop response of active feedback control of the 2/1 mode at moderate gain was observed to be in good agreement with the theory and the phase angle of the applied field was varied relative to the 2/1 island. However, at high system gain stable phase control was not achieved and a higher digitization rate and faster digital signal processing system will be necessary. As a consequence effect on the disruption process through control of the 2/1 island amplitude have not yet been demonstrated for this mode control technique.

Experiments have been carried out which show suppression of the 2/1 island growth using an asynchronous frequency modulation drive which maintains the ion inertial effect of flow damping. Originally suggested and modeled by Kurita, at al.[17] we apply asynchronous external control fields at frequencies alternately above and below the natural mode frequency. Previous experiments have not had the capability to modulate the frequency of the rotating mode sufficiently fast to observe significant damping from this flow stabilizing effect. The frequency modulation control technique was also able to

prevent disruptions normally observed to follow giant sawtooth crashes in the plasma core. By preventing the uncontrolled growth of the 2/1 island following a large sawtooth as normally occurs, the confinement of the outer flux surfaces was preserved and the disruption was prevented allowing the plasma core to re-heat.

ACKNOWLEDGMENTS

The research here is supported by DOE Grant DE-FG02-86ER53222. The authors also gratefully acknowledge the technical support provided by M. Cea, N. Rivera, and E. Rodas.

---

[1] E. A. Lazarus, G. A. Navratil, *et al. Phys Rev Lett* **77** (1996) 2714.
[2] C. Kessel, J. Manickam, G. Rewoldt, and W. Tang, *phys Rev lett* **72** (1994) 1212 and J. Manickam, M. S. Chance, S. C. Jardin, *et al.*, *Physics of Plasmas* **1** (1994) 1601.
[3] A. Turnbull, *et al.*, PRL **74** (1995) 718.
[4] T. Taylor, E. J. Strait, L.L. Lao, M. Mauel, *et al.*, Phys. Plasmas **2** (1995) 2390.
[5] T. Ivers, E. Eisner, A. Garafalo, R. Kombargi, M. E. Mauel, *et al.*, Phys. Plasmas **3** (1996) 1926.
[6] F. Freidberg, *Ideal Magnetohydrodynamics*, Plenum Press (New York, 1987).
[7] David A. Gates, "Passive Stabilization of MHD Instabilities at High β_N in the HBT-EP Tokamak", Columbia University Ph.D. Thesis 1993, Columbia Plasma Physics Laboratory Report No. 107.
[8] E. Lazzaro and M. F. F. Nave, *Phys. Fluids* **31** (1988) 1623.
[9] A. W. Morris, *et al.*, *Phys Rev Lett* **64** (1990) 1254.
[10] G. Bosia and E. Lazzaro, *Nucl. Fusion* **31** (1991) 1003.
[11] G. D'Antonia, IEEE *Trans Nucl Sci* **41** (1994) 216.
[12] A. I. Smolyakov, A. Hirose, E. Lazzaro, G. B. Re, and J. D. Callen, *Phys Plasmas* **2** (1995) 1581.
[13] T. C. Hender, R. Fitzpatrick, A. W. Morris, P. G. Carolan, R. D. Durst,*et al.*, *Nucl. Fusion* **32** (1992) 2091.
[14] K. Oasa, H. Aikawa, Y. Asahi, K. Hoshino, *et al. Plasma Phsyics and Controlled Nuclear Fusion Research 1994*, Seville, 1994. (International Atomic Energy Agency, Vienna, 1995) Vol. 2, p 279.
[15] E. Lazzaro and M.F.F. Nave, *Phys. Fluids* **31** (1988) 1623.
[16] G. Bosia and E. Lazzaro, *Nucl. Fusion* **31** (1991) 1003.
[17] G. Kurita, T. Tuda, M, Azumi, and T. Takeda, *Nucl. Fusion* **32** (1992) 1899.

Figure Captions

Figure 1. Schematic of the HBT-EP control coil configuration showing ten 26° wide conducting wall segments with 6° wide m=2 saddle coils located at 4 of the 10° wide gaps in the conducting wall segments. A sin2θ and cos2θ Rogowski coil quadrature detector is located to be physically remote from the saddle coils.

Figure 2. Schematic of the closed lop system for mode control on HBT-EP consisting of a digital signal processor which produced a phase and gain adjusted output into two 10 MW linear amplifiers which generate a sin and cosine phase for the saddle coil generated rotating 2/1 response field.

Figure 3. Frequency ramp up experiment from 2 kHz to 15 kHz showing the applied and plasma 2/1 mode field, the phase of the 2/1 mode relative to the phase of the applied field, and the frequency of the applied field and the 2/1 mode as a function of time.

Figure 4. Model calculation for a frequency ramp-up experiment with and without inclusion of the flow damping term in the model equations showing the time evolution of the applied and m2/1 mode frequency and the applied and 2/1 mode amplitude.

Figure 5. Local measurement of the ion flow velocity with a Langmuir Mach probe during a frequency ramp-up and ramp down experiment.

Figure 6 Measurement of the phase instability when the toroidal phase of a rotating magnetic perturbation is suddenly advanced by 180°. The time history of the

measured amplitude and phase of the 2/1 island is shown compared with simulation calculations with and without the flow damping term in the model equations.

Figure 7 Results of the equilibrium model calculations Eqs. (4) and (5) as a function of phase angle for moderate gain.

Figure 8 Application of stabilizing (0°) phase and destabilizing (180°) phase each for 1 msec compared with the results of the equilibrium model shown in Fig. 7.

Figure 9 Application of frequency downshift (270°) phase and frequency upshift (90°) phase each for 1 msec compared with the results of the equilibrium model shown in Fig. 7.

Figure 10 Simulation of the effect on the mode amplitude and mode frequency in response to frequency modulation of the applied field with 5 kHz and 15 kHz applied for 0.2 msec alternately. The simulation illustrates the result of including the effect of flow damping in the model equations.

Figure 11 Results of experiment using frequency modulation of the applied field with 5 kHz and 15 kHz applied for 0.2 msec alternately. The squared frequency modulation $(\Omega\text{-}1)^2$ is compared with the mode amplitude.

Figure 12 Disruption control demonstration of frequency modulation suppression comparing a disruptive reference shot 16389 to a similar shot with FM suppression does not disrupt in response to a large sawteeth event.

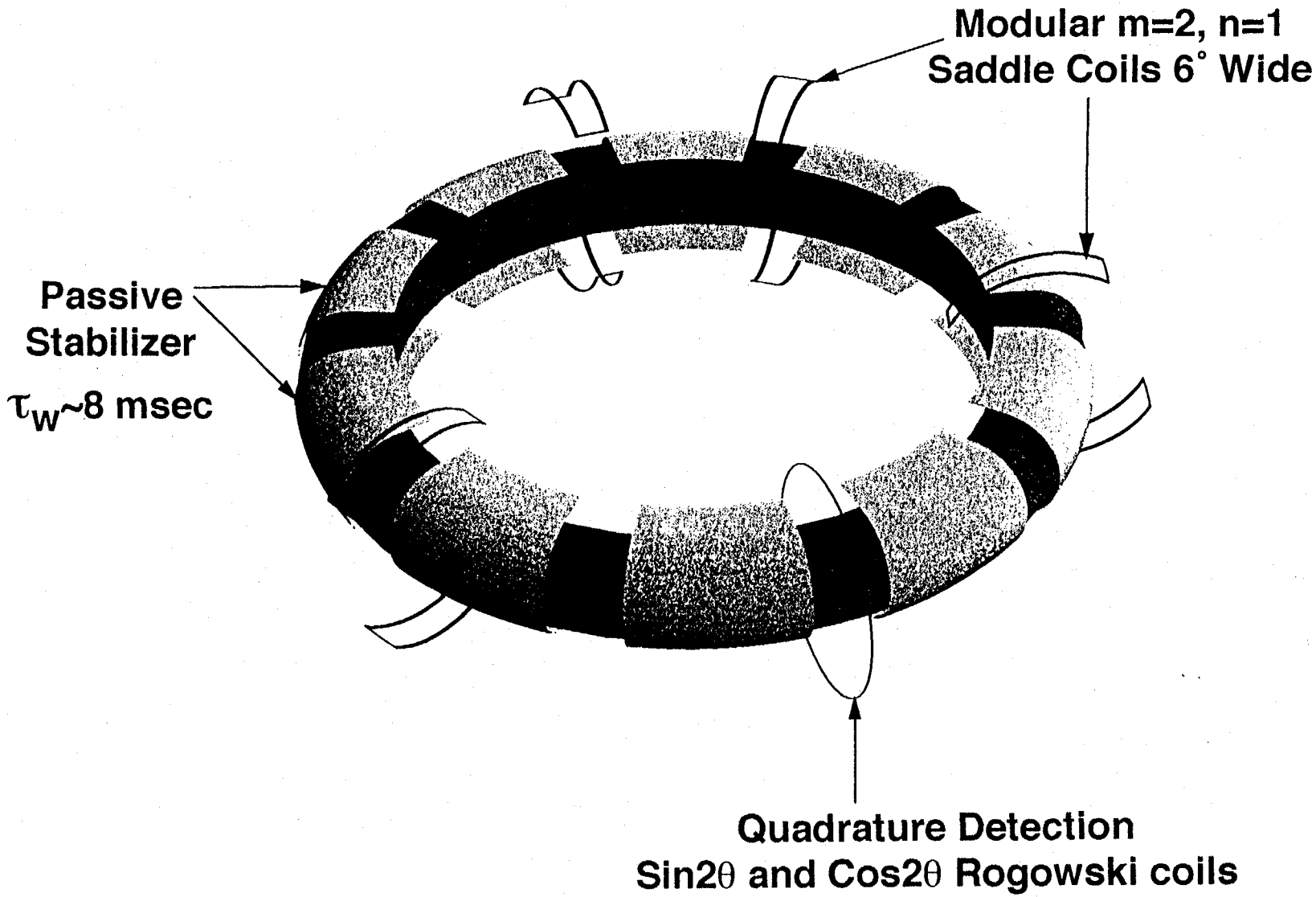
Modular m=2, n=1
Saddle Coils 6° Wide
Passive
Stabilizer
τ_W~8 msec
Quadrature Detection
Sin2θ and Cos2θ Rogowski coils

Fig. 1

Fig. 2

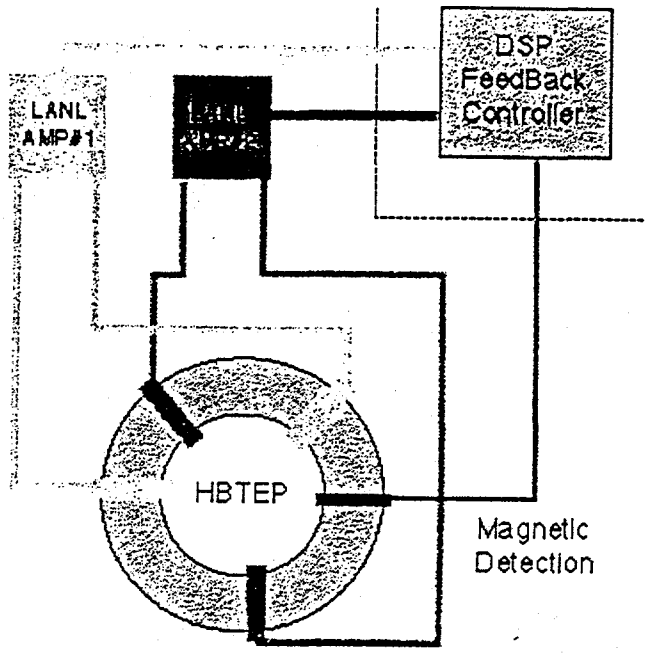
DSP
FeedBack
Controller
LANL
AMP#1
HBTEP
Magnetic
Detection

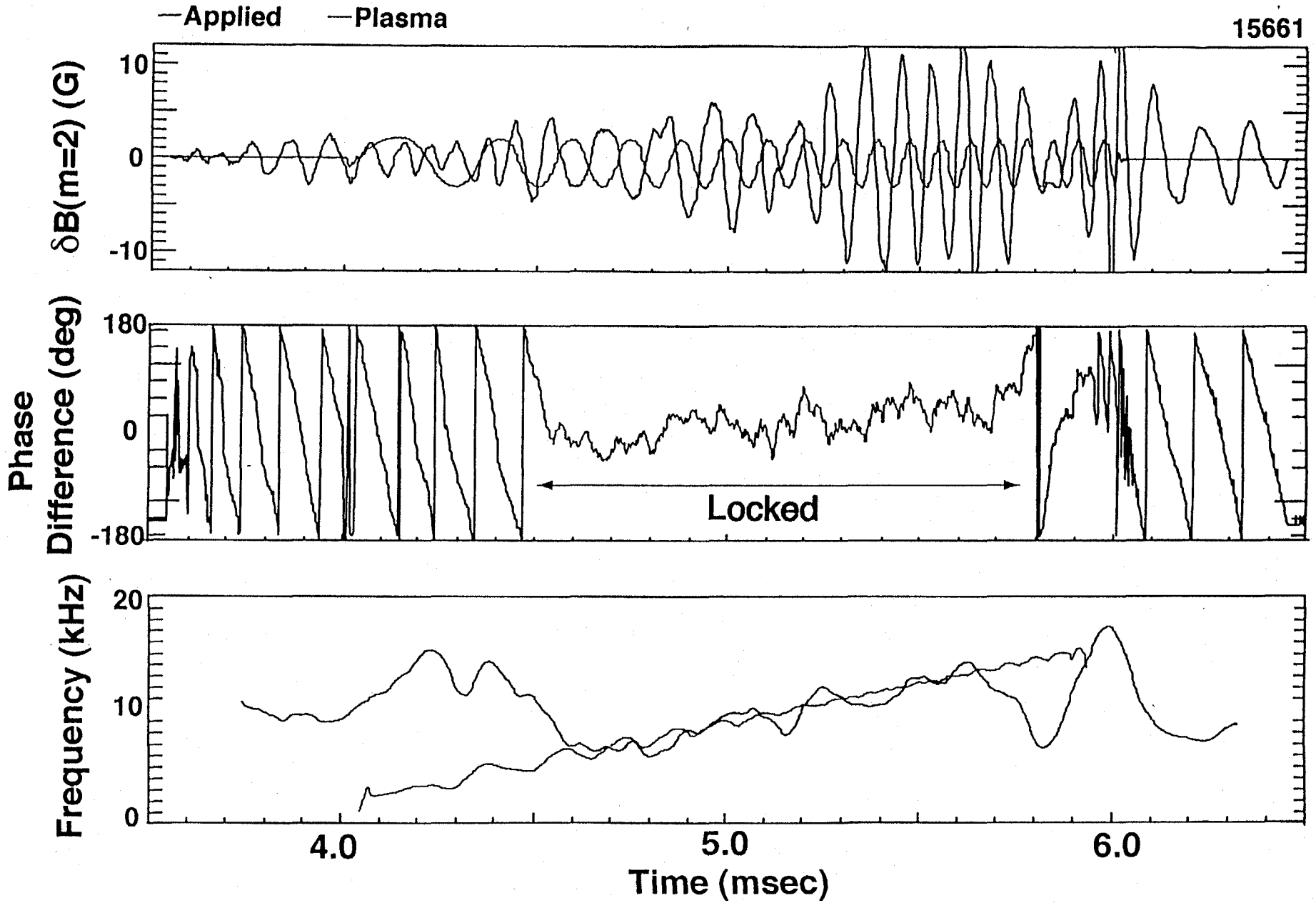
—Applied
—Plasma
15661
δB(m=2) (G)
10
0
-10
Phase Difference (deg)
180
0
-180
Locked
Frequency (kHz)
20
10
0
4.0
5.0
6.0
Time (msec)

Fig. 3

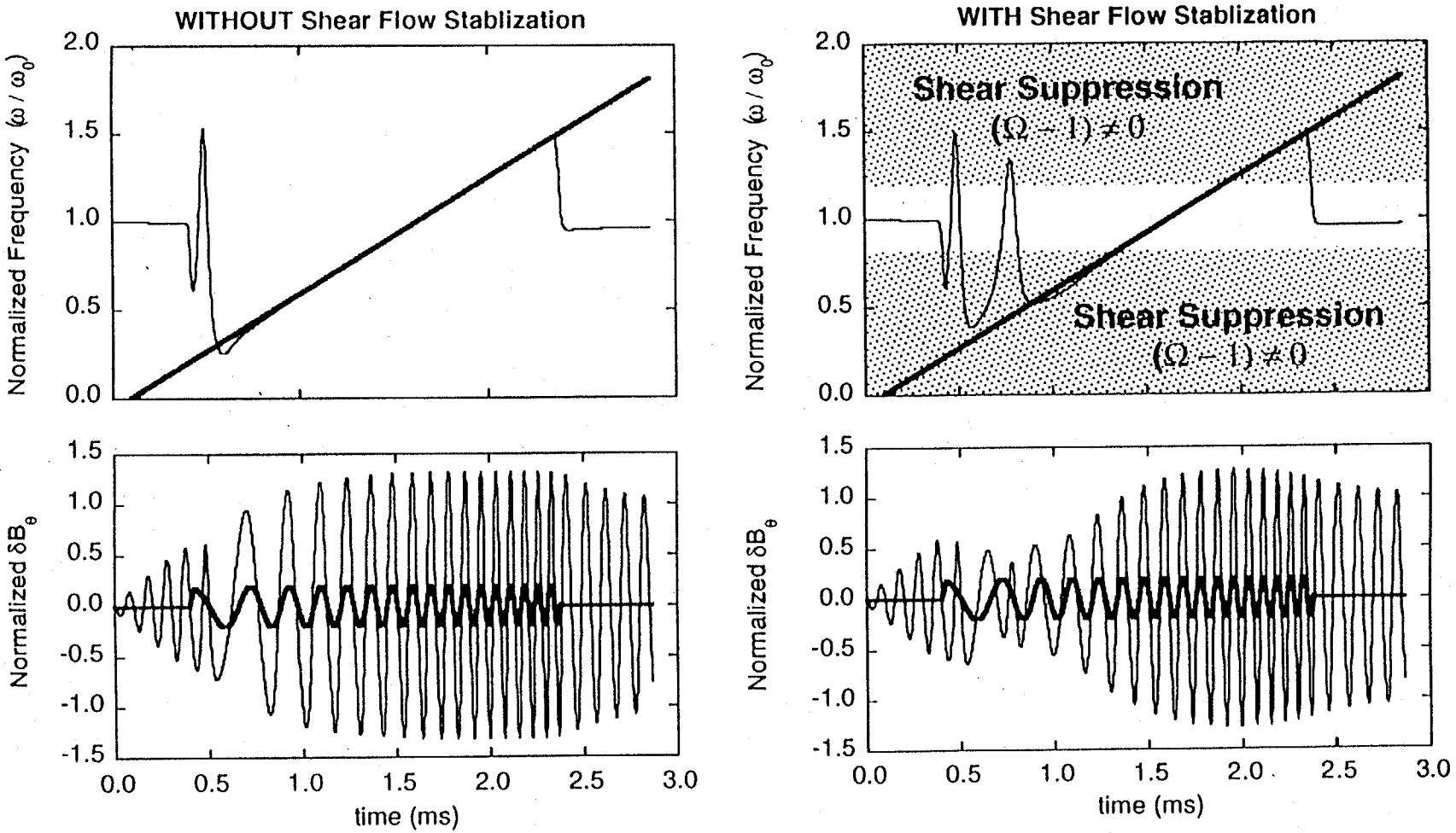
WITHOUT Shear Flow Stablization
WITH Shear Flow Stablization
Normalized Frequency (ω / ω0)
Normalized δBθ
Shear Suppression
(Ω − 1) ≠ 0
Shear Suppression
(Ω − 1) ≠ 0
time (ms)
time (ms)

Fig. 4

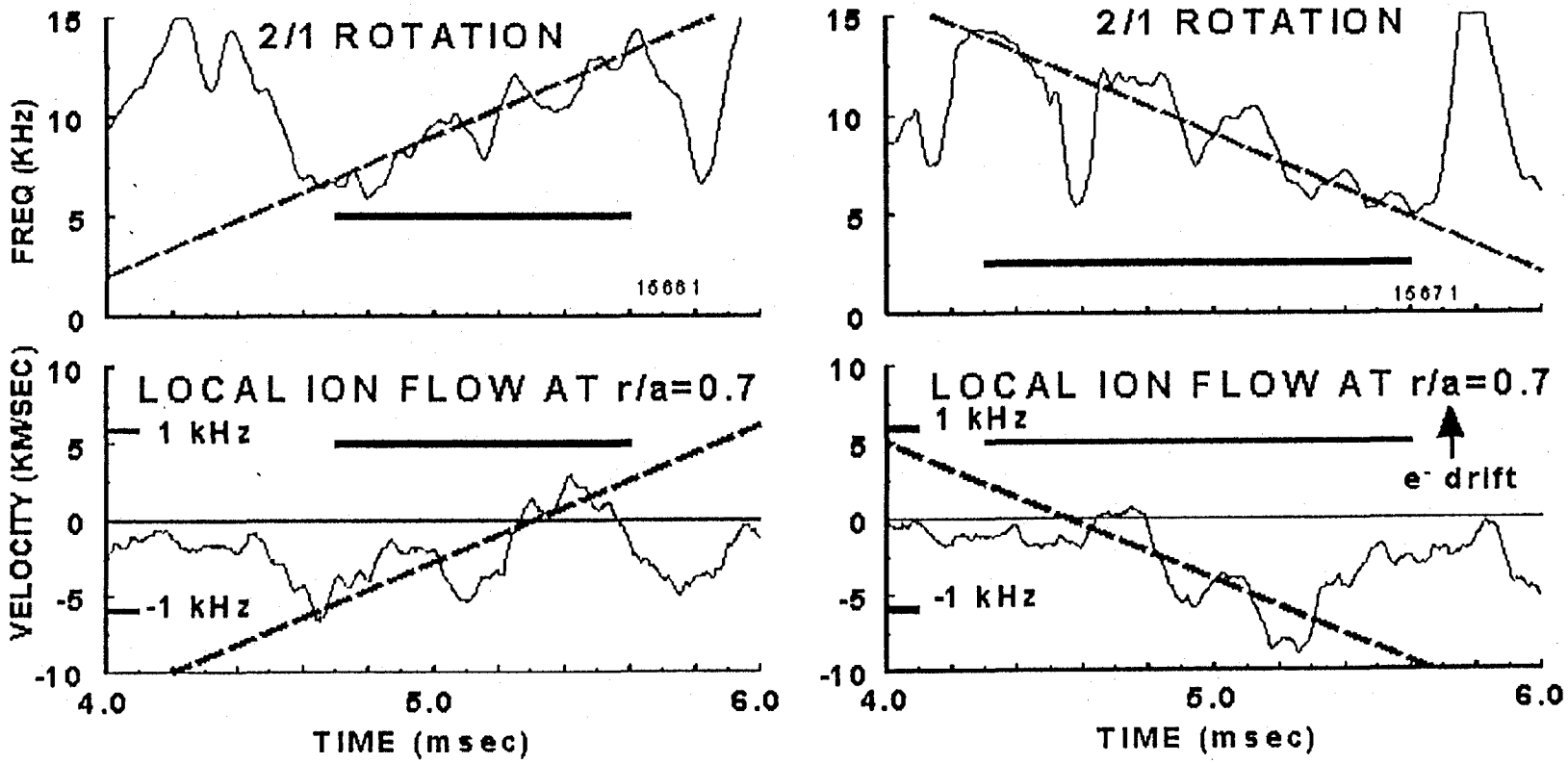
2/1 ROTATION
FREQ (KHz)
15
10
5
0
15661
2/1 ROTATION
15671
LOCAL ION FLOW AT r/a=0.7
1 kHz
-1 kHz
VELOCITY (KM/SEC)
10
5
0
-5
-10
4.0
5.0
6.0
TIME (msec)
LOCAL ION FLOW AT r/a=0.7
1 kHz
e⁻ drift
-1 kHz
TIME (msec)

Fig. 5

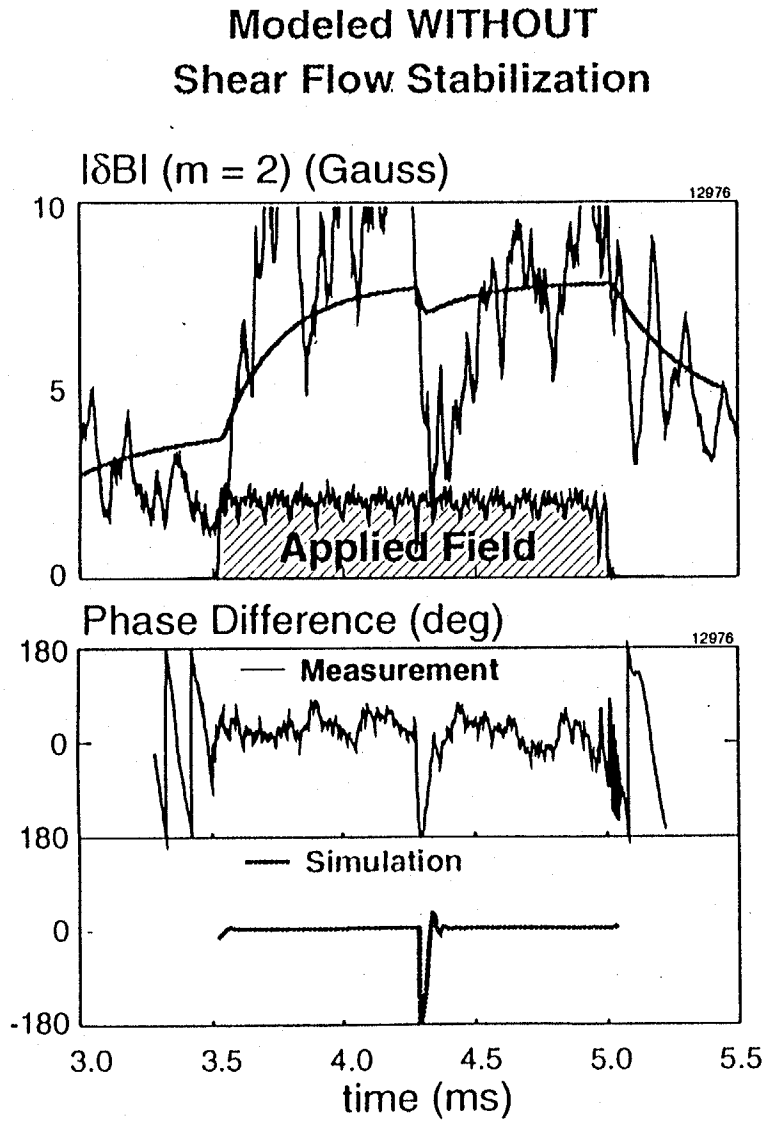
Modeled WITHOUT
Shear Flow Stabilization
|δB| (m = 2) (Gauss)
12976
10
5
0
Applied Field
Phase Difference (deg)
12976
180
0
180
0
-180
Measurement
Simulation
3.0
3.5
4.0
4.5
5.0
5.5
time (ms)

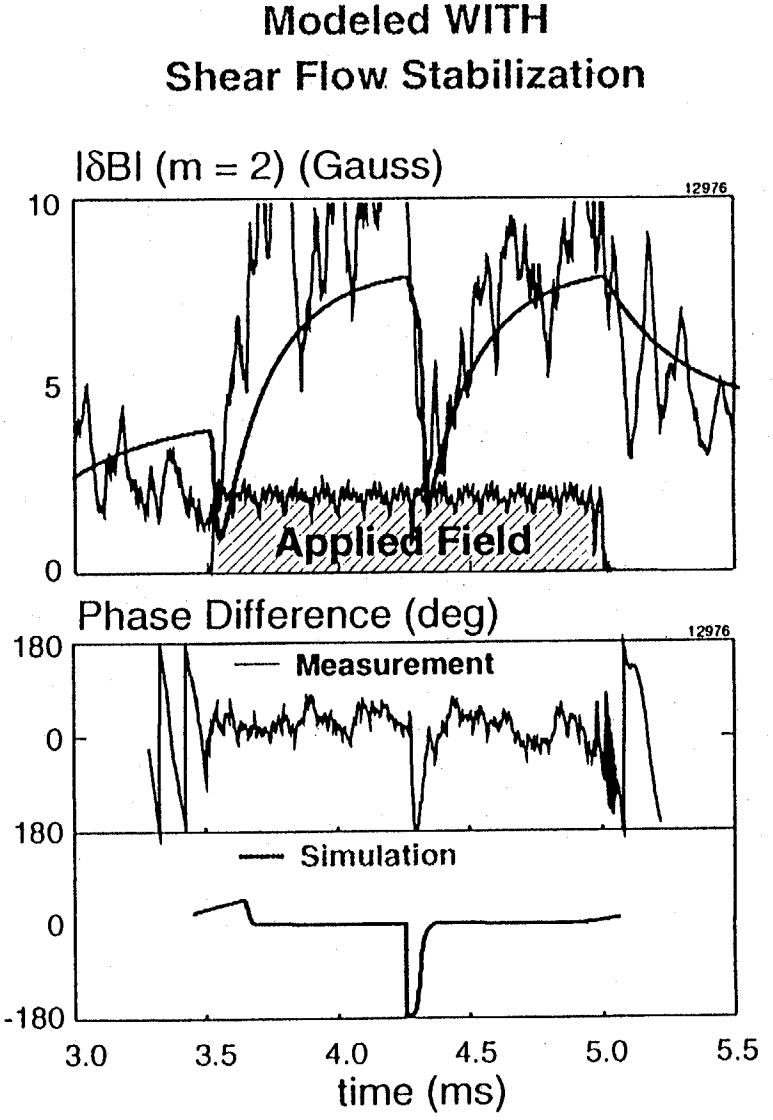
Modeled WITH
Shear Flow Stabilization
|δB| (m = 2) (Gauss)
12976
10
5
0
Applied Field
Phase Difference (deg)
12976
180
0
180
0
-180
Measurement
Simulation
3.0
3.5
4.0
4.5
5.0
5.5
time (ms)

FIG. 6

Normalized Mode Amplitude

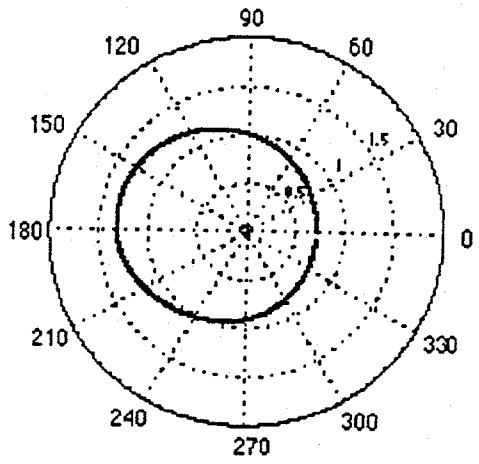

Normalized Mode Frequency

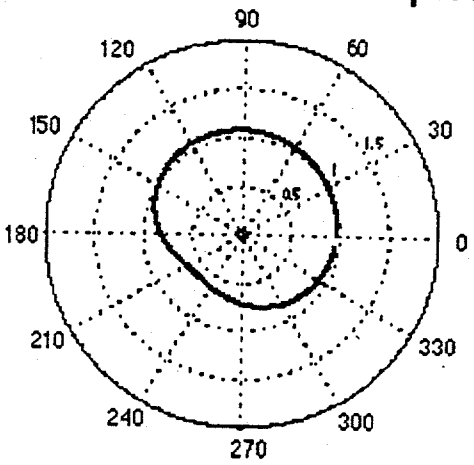

Phase Angle δ

Fig 7

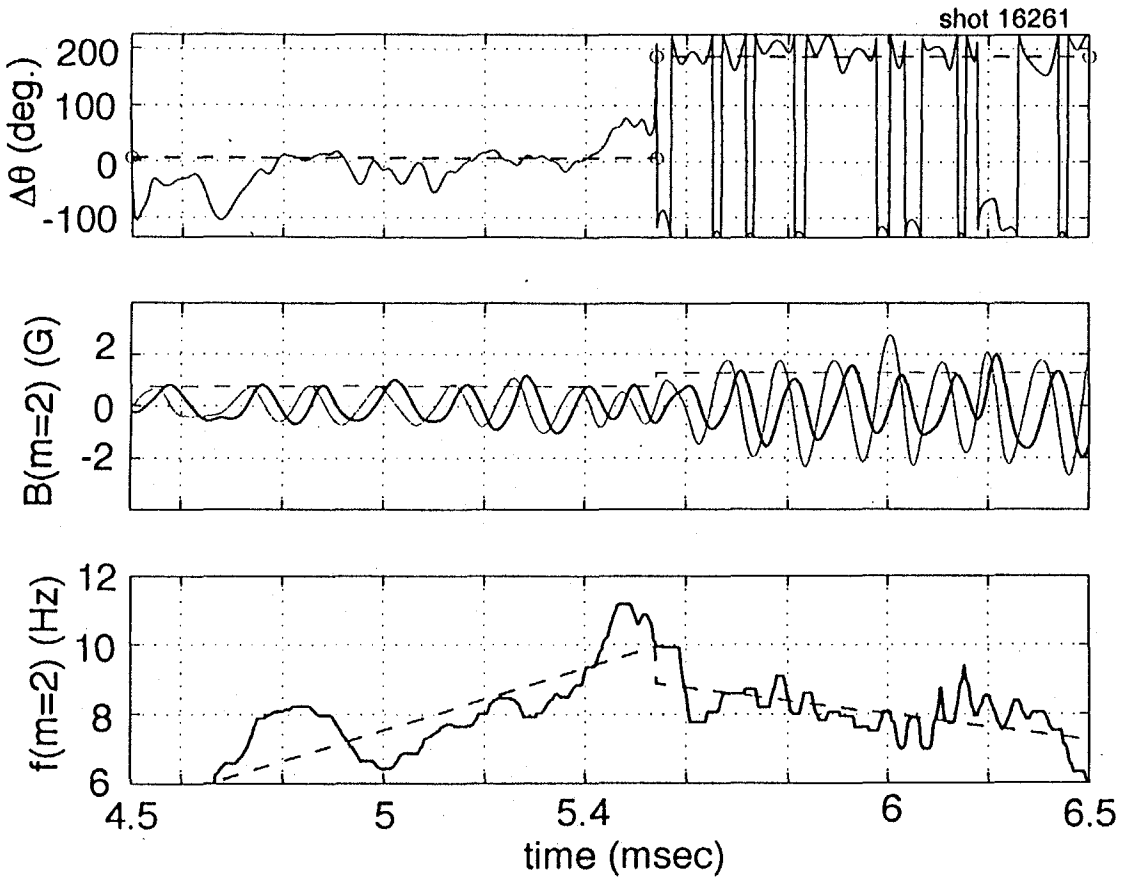

Normalized Mode Amplitude

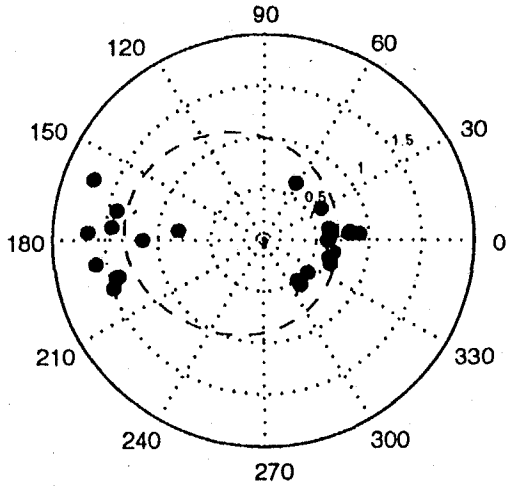

Normalized Mode Frequency

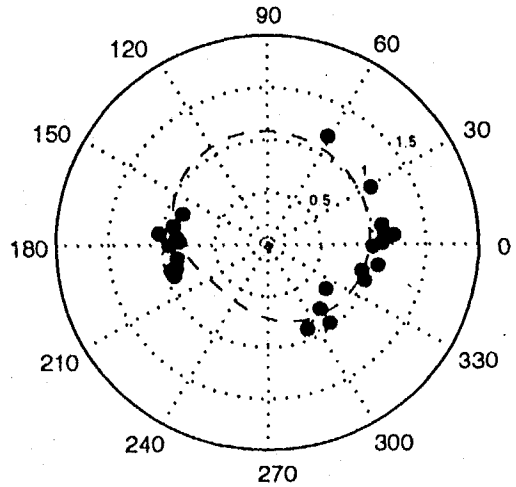

Δθ Phase Angle

Fig. 8

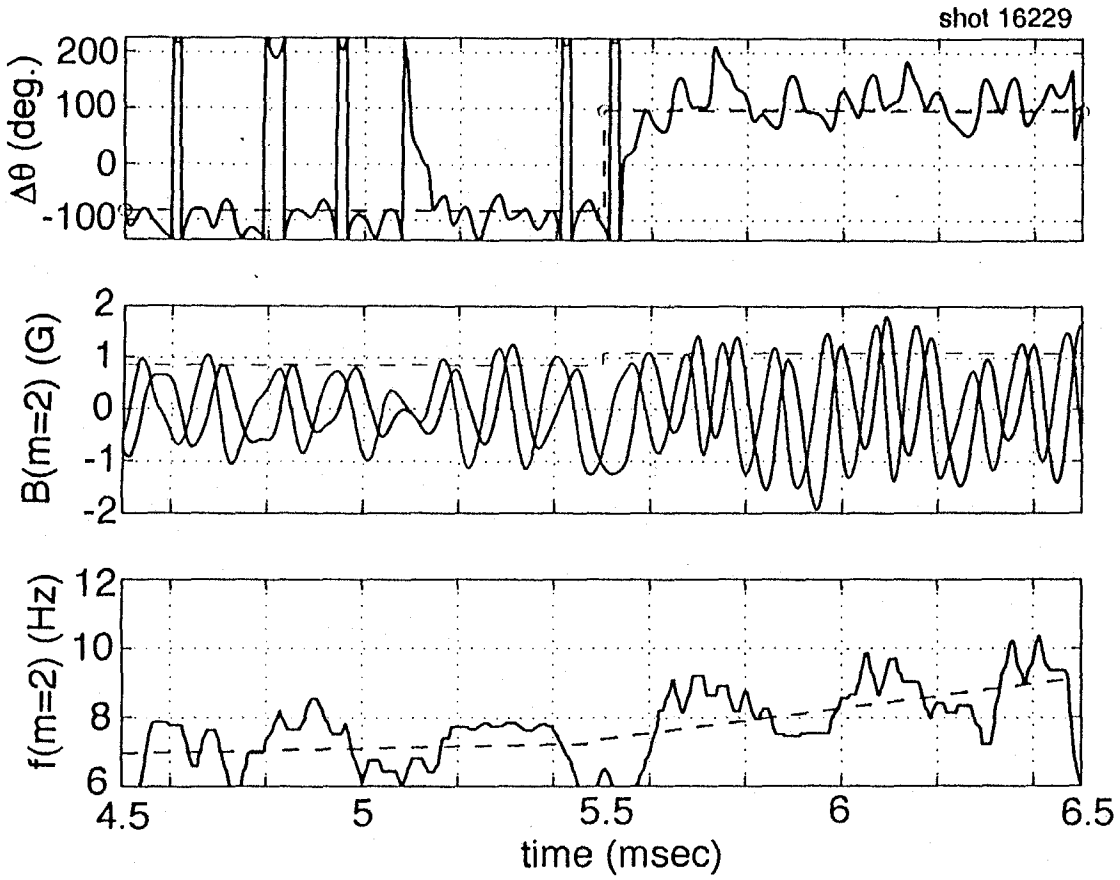

Normalized Mode Amplitude

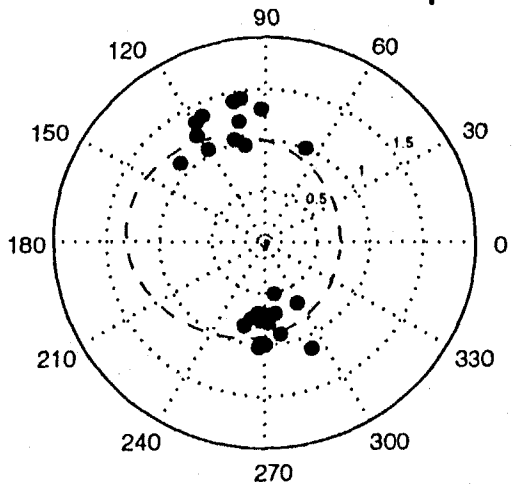

Normalized Mode Frequency

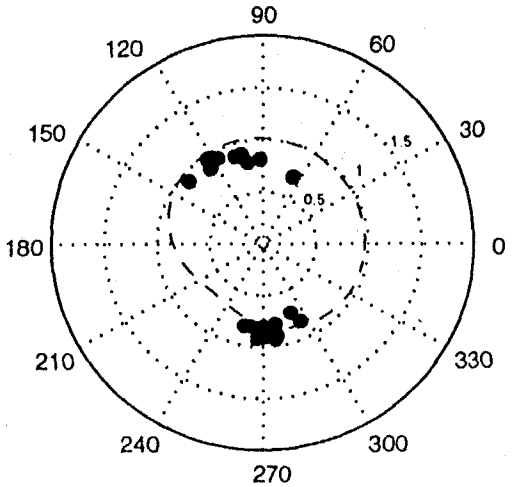

Δθ Phase Angle

Fig 9

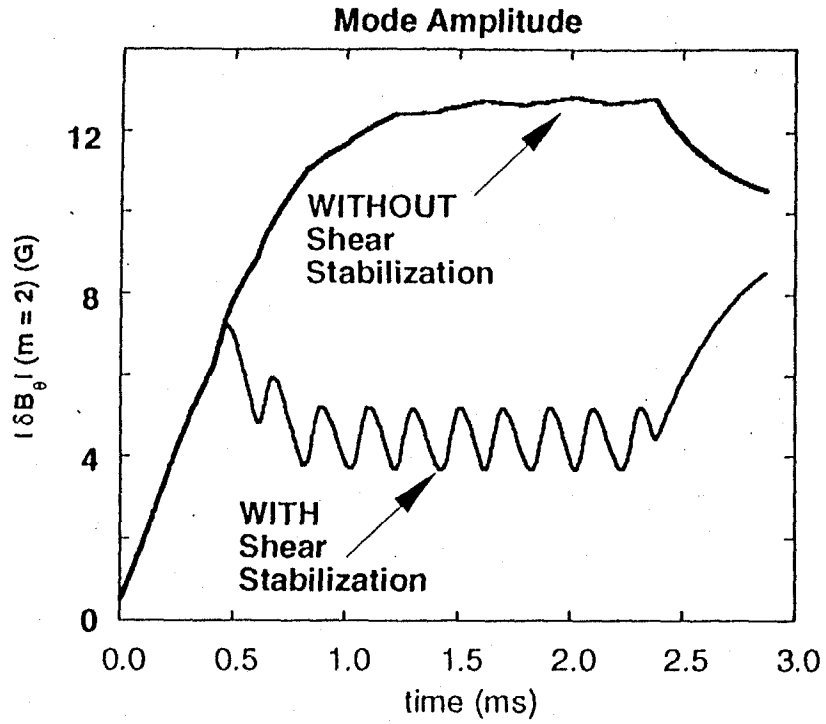
Mode Amplitude
12
8
4
0
WITHOUT
Shear
Stabilization
WITH
Shear
Stabilization
0.0
0.5
1.0
1.5
2.0
2.5
3.0
time (ms)
|δB_θ| (m = 2) (G)

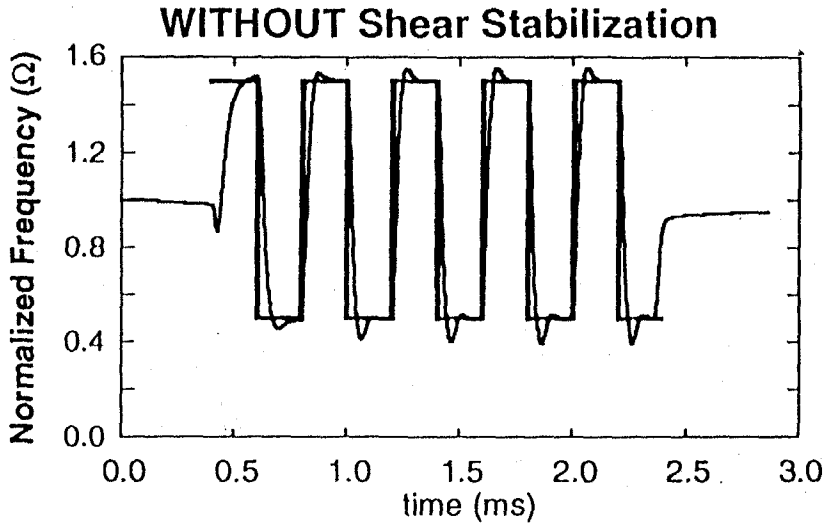
WITHOUT Shear Stabilization
1.6
1.2
0.8
0.4
0.0
Normalized Frequency (Ω)
0.0
0.5
1.0
1.5
2.0
2.5
3.0
time (ms)

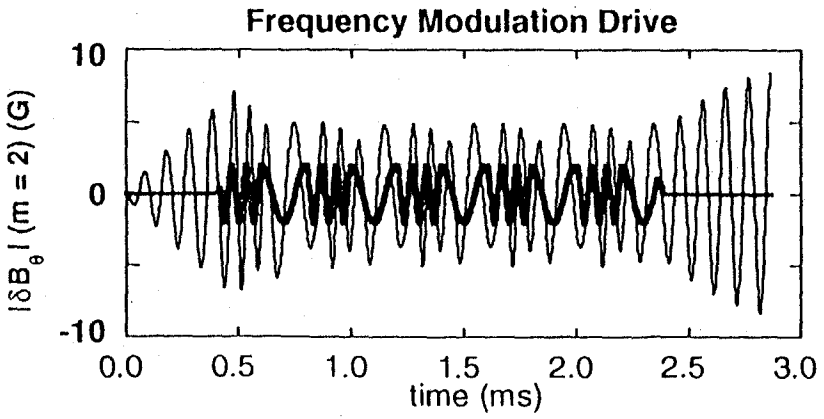
Frequency Modulation Drive
10
0
-10
|δB_θ| (m = 2) (G)
0.0
0.5
1.0
1.5
2.0
2.5
3.0
time (ms)

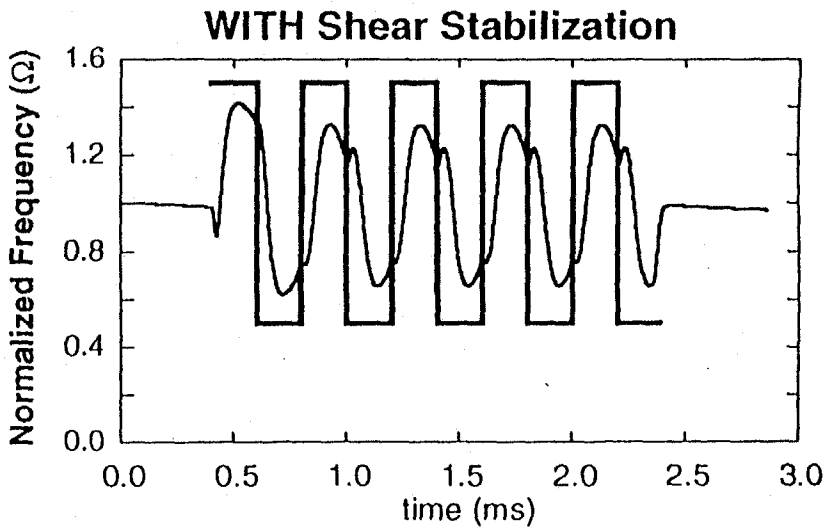
WITH Shear Stabilization
1.6
1.2
0.8
0.4
0.0
Normalized Frequency (Ω)
0.0
0.5
1.0
1.5
2.0
2.5
3.0
time (ms)

Fig 10

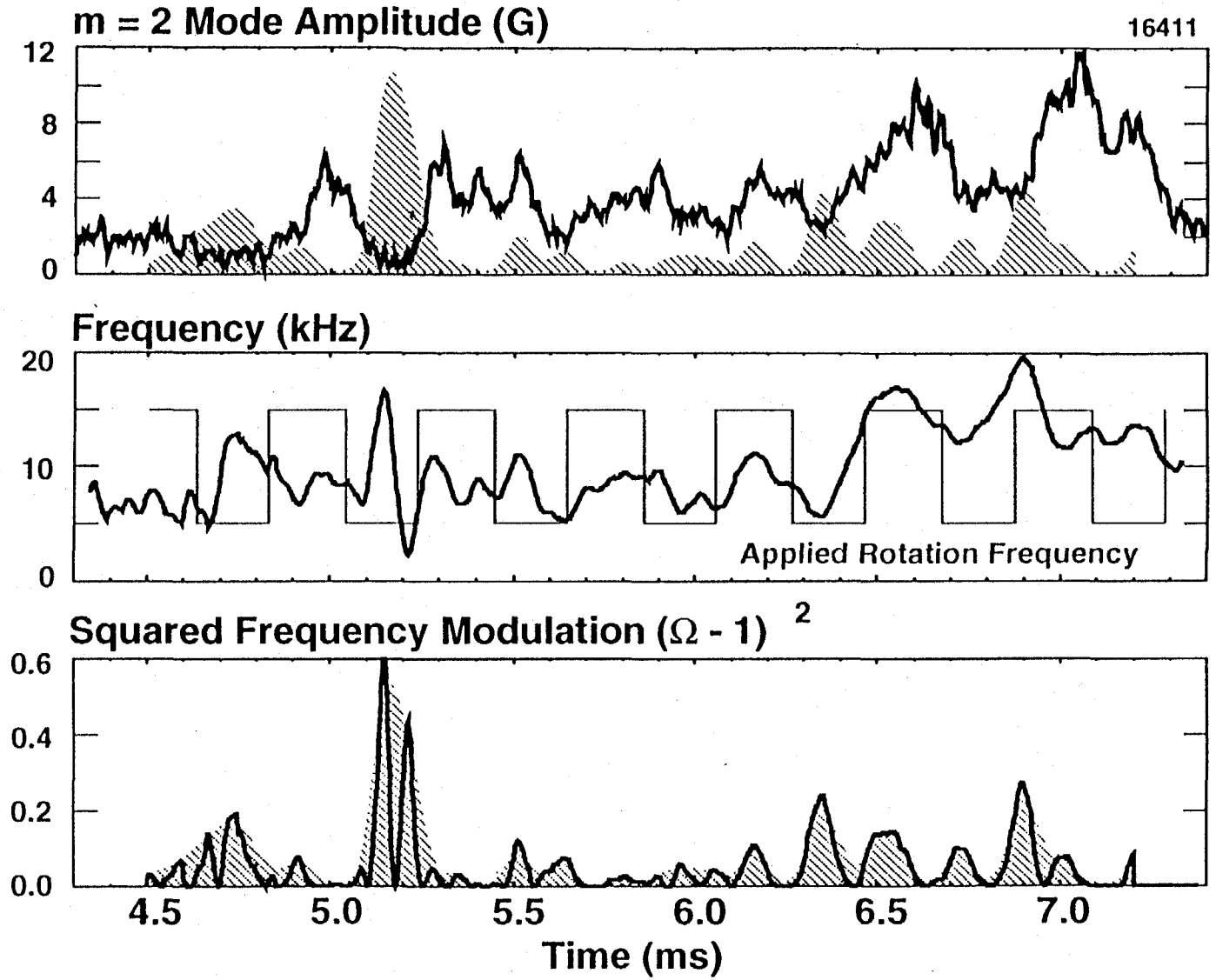
m = 2 Mode Amplitude (G)
16411
12
8
4
0
Frequency (kHz)
20
10
0
Applied Rotation Frequency
Squared Frequency Modulation (Ω - 1) 2
0.6
0.4
0.2
0.0
4.5
5.0
5.5
6.0
6.5
7.0
Time (ms)

FIG. 11

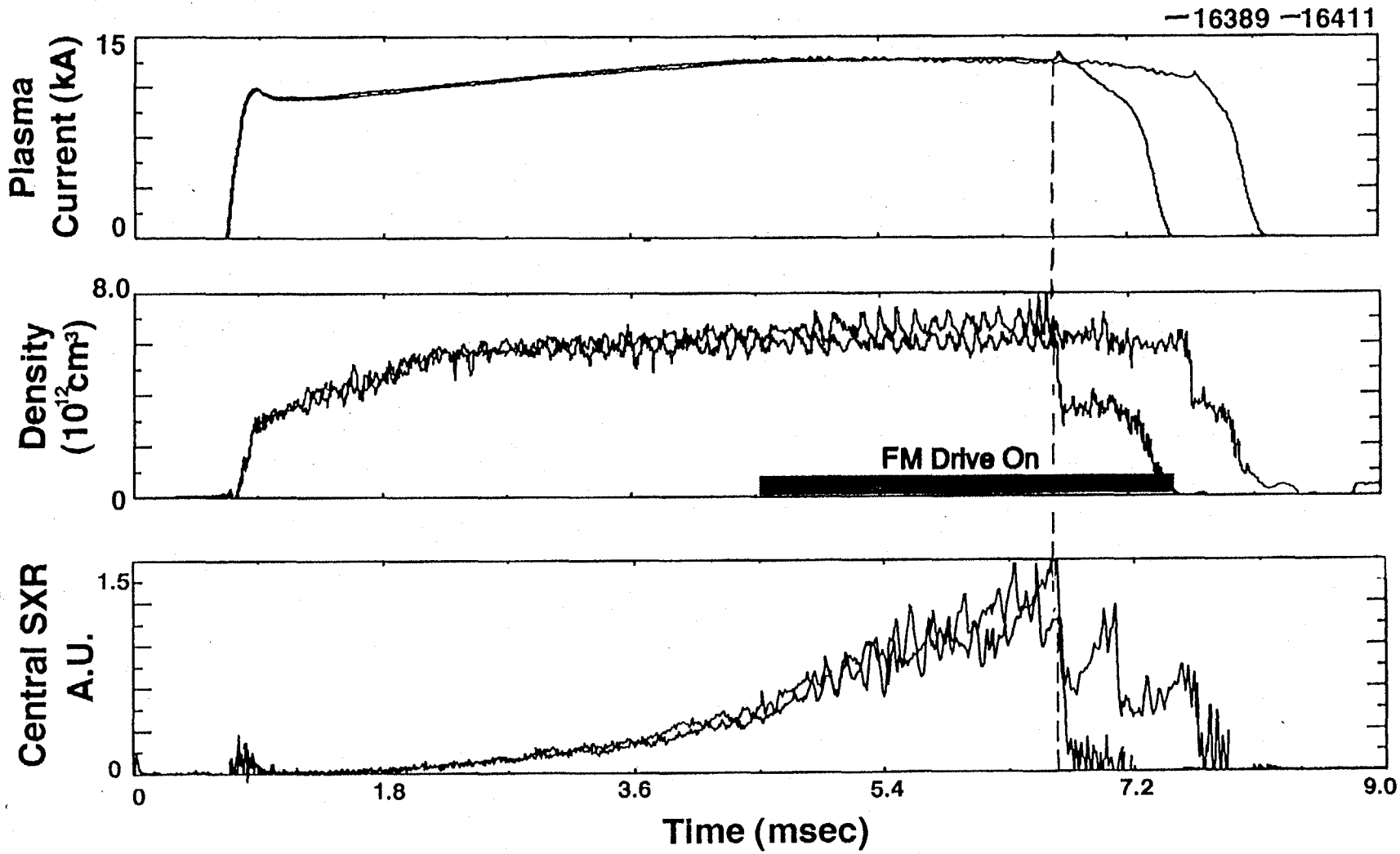
—16389 —16411
Plasma Current (kA)
15
0
Density (10^{12}cm^3)
8.0
0
FM Drive On
Central SXR A.U.
1.5
0
0
1.8
3.6
5.4
7.2
9.0
Time (msec)

FIG. 12